Catalysis Science & Technology

PAPER

Check for updates

Cite this: *Catal. Sci. Technol.*, 2017, 7, 2789

Oxidation of the hexagonal $Mo_2C(101)$ surface by H_2O dissociative adsorption†

Xinxin Tian,[a] Tao Wang[b] and Haijun Jiao *[c]

Received 13th April 2017,
Accepted 21st May 2017

DOI: 10.1039/c7cy00728k

rsc.li/catalysis

Oxidation of the hexagonal $Mo_2C(101)$ surface by H_2O dissociative adsorption was investigated using periodic density functional theory. At coverage (θ_{H_2O}) up to 0.5 ML, all H_2O molecules adsorb on the top of surface Mo_A atoms, while further H_2O adsorption relies only on hydrogen bonding at $\theta_{H_2O} > 0.5$ ML. Up to 0.5 ML coverage, H_2O dissociation into surface OH is very facile and exothermic, and the dissociation of OH into O + H can establish equilibrium. Surface O can easily react with H_2O to generate surface OH. The most abundant oxygenate species on $Mo_2C(101)$ should be surface OH instead of surface O atoms. The highest coverage of surface OH is 0.5 ML. These results provide new insight into the understanding of surface compositions on Mo_2C under an H_2O environment, and surface OH rather than surface O atoms should play an essential role in mechanisms of many related reactions.

1. Introduction

Molybdenum-based Mo_2C, Mo_2N, MoS_2 and MoP materials represent a set of promising heterogeneous catalysts in industrial hydro-treating processes.[1,2] It has been long proved that Mo_2C and W_2C are noble metal-like in hydrogenation reactions[3,4] and very good candidates to substitute for noble metal-based catalysts. On the basis of the promising catalytic properties of Mo_2C, extensive experimental investigations into the water-gas shift (WGS) reaction,[5,6] hydro-treating,[7] hydrodesulfurization,[8] hydrodenitrogenation,[9] hydrogen production,[10] alcohol synthesis from CO hydrogenation[11] and hydrodeoxygenation of biomass[12–16] have been reported. Mo_2C is also found to be a very promising and active catalyst in the hydrogen evolution reaction.[17–22] Molybdenum carbides mainly have orthorhombic and hexagonal Mo_2C phases with Mo/C = 2/1 as well as a face-centered cubic MoC phase with Mo/C = 1/1;[23] all these phases have been considered as catalysts. Mo_2C has been also found to play the roles of both support and active site in noble-metal/Mo_2C systems as novel catalysts for CO oxidation, desulfurization and hydrogenation reactions.[24,25] Supported (Au,Cu)/δ-MoC[26] and Cu/Mo_2C[27] are found to be very promising catalysts for CO_2 conversion and their activity is affected by the carbon/metal ratio of molybdenum carbides.[28] Recently, Ma *et al.*[29] have successfully synthesized a highly efficient and stable Cu/hexagonal-Mo_2C catalyst for the reverse water gas shift (RWGS) reaction. Since traditional Cu-oxide catalysts tend to be deactivated dramatically in the RWGS reaction because of the aggregation of supported copper particles at high temperatures, hexagonal Mo_2C as a typical kind of transition metal carbide has been demonstrated to be capable of dispersing and stabilizing copper particles. Cu/hexagonal-Mo_2C catalysts exhibit excellent catalytic activity and stability for the RWGS reaction.

Since H_2O is involved in these reactions as either a reactant or a product, understanding the interaction of H_2O with Mo_2C catalysts has many interesting scientific aspects, *e.g.* the surface structure of Mo_2C and the stable states of the adsorbed H_2O. Actually, Mo_2C can be easily oxidized by H_2O, O_2 and CO_2.[30] Recent work by Chen and Bhan[31] showed that O_2-pretreated Mo_2C catalysts have a 10-fold decrease in toluene synthesis rate compared with freshly prepared as well as H_2O and CO_2-pretreated Mo_2C catalysts. They proposed that O_2 can poison the metal-like sites which are responsible for the formation of *m*-cresol. Thus, identifying the surface structure and composition of Mo_2C under an H_2O environment is essential for rational understanding of its reaction mechanisms, and theoretical studies can play an important role in describing the surface compositions of catalysts and their reaction mechanisms on an atomic scale.

Although extensive theoretical investigations into the properties of Mo_2C catalysts are readily available, *e.g.* the adsorption of CO,[32–37] H_2,[38–41] thiophene,[42] indole,[43] methanol[44]

[a] *Key Laboratory of Materials for Energy Conversion and Storage of Shanxi Province, Institute of Molecular Science, Shanxi University, Taiyuan 030006, China*

[b] *Laboratoire de Chimie, Université Claude Bernard Lyon 1, CNRS UMR 5182, Ens de Lyon, Univ Lyon, F69342, Lyon, France*

[c] *Leibniz-Institut für Katalyse e.V. an der Universität Rostock, Albert-Einstein Strasse 29a, 18059 Rostock, Germany. E-mail: haijun.jiao@catalysis.de*

† Electronic supplementary information (ESI) available: Energetic data for dissociation of nH_2O on the $Mo_2C(101)$ surface; the detailed H-bond arrangement at different H_2O coverages; structures of IS, TS and FS for H_2O dissociation at different coverages. See DOI: 10.1039/c7cy00728k

and methyl iodide[45] and their reaction mechanisms,[46–50] H_2O adsorption and dissociation on Mo_2C surfaces were barely investigated, apart from some primary steps during previous mechanistic studies. In studies of the mechanisms of the water-gas shift reaction, for example, Tominaga *et al.*[51] and Liu *et al.*[52] proposed that H_2O can dissociate into OH and H very favorably on the Mo_2C catalyst, and CO_2 formation from CO oxidation by surface O is the rate-determining step. In their activation mechanism investigations into small molecules, Shi *et al.*[53–55] found low energy barriers for H_2O dissociation on Mo_2C(001) and (101) surfaces. It should be noted that all these very limited studies focused only on the properties of a single H_2O molecule, and did not touch the cases with certain H_2O molecules.

In this respect, systematic theoretical investigations into the high coverage adsorption of H_2O as well as the oxidation of the Mo_2C surface are highly desired. Thus, we performed a DFT study of H_2O adsorption and dissociation on the hexagonal Mo_2C(101) surface at different coverages to identify the stable composition of the Mo_2C surface under experimentally relevant conditions.

2. Computational model and method

2.1 Method

The plane-wave-based periodic density functional theory method implemented in the Vienna *ab initio* simulation package (VASP)[56–58] was used for all calculations. The electron–ion interaction was described with the projector augmented wave method.[59] The electron exchange and correlation energy was treated within the generalized gradient approximation in the Perdew–Burke–Ernzerhof formalism (GGA-PBE).[60] The cutoff energy of 400 eV and the Gaussian electron smearing method with σ = 0.05 eV were used. Geometry optimization was performed when the convergence criterion on forces became smaller than 0.02 eV Å^{-1} and the energy difference was lower than 10^{-4} eV. The adsorption energy (E_{ads}) of one H_2O molecule is calculated using $E_{ads} = E(H_2O/slab) - E(H_2O) - E(slab)$, where $E(H_2O/slab)$ is the total energy of the slab with adsorbed H_2O molecules in its equilibrium geometry, $E(H_2O)$ is the total energy of H_2O in the gas phase, and $E(slab)$ is the total energy of the clean surface. A more negative E_{ads} indicates more stable adsorption. At high coverage, the stepwise adsorption energy ($\Delta E_{ads} = E[(H_2O)_{n+1}/slab] - E[(H_2O)_n/slab] - E[H_2O]$) was used. To evaluate the energy barrier ($E_a = E_{TS} - E_{IS}$), the transition state (TS) was located using the Nudged Elastic Band (NEB) method.[61] All transition states were verified by vibration analyses with only one imaginary frequency. The adsorption energy (E_{ads}) of OH and O species is calculated using $E_{ads}(OH)_n = E(OH_n/slab) + n/2E(H_2) - nE(H_2O) - E(slab)$ or $E_{ads}(O)_n = E(O_n/slab) + nE(H_2) - nE(H_2O) - E(slab)$, where n is the number of adsorbents, $E(OH_n/slab)$ is the total energy of the slab with n adsorbed OH groups, $E(O_n/slab)$ is the total energy of the slab with n adsorbed O atoms, and $E(H_2)$ is the total energy of H_2 in the gas phase. Unless otherwise mentioned, all reported energetic data include zero-point energy (ZPE) correction, while those without ZPE correction are listed in the ESI† for comparison.

2.2 Model

In this work, we applied the hexagonal phase of Mo_2C,[62] where the (101) surface is the most stable and dominant on the basis of the computed surface free energies from the atomistic thermodynamic method,[63] in agreement with experiment. The calculated lattice parameters for bulk hexagonal Mo_2C (a = 6.075 Å, b = 6.069 Å, c = 4.722 Å) are in agreement with experiment ($a = b = 2 \times 3.011$ Å, c = 4.771 Å).[64] A $p(2 \times 1)$ supercell with a thickness of 5.94 Å was chosen to model the (101) surface, where the top 3.54 Å were allowed to relax and the bottom 2.40 Å were fixed in their bulk positions. The vacuum layer thickness between periodically repeated slabs was set to 12 Å to avoid interactions between slabs. The entire supercell contains a $Mo_{32}C_{16}$ unit.

On the $p(2 \times 1)$ Mo/C-mixed Mo_2C(101) surface (Fig. 1), there are eight surface Mo and eight surface C atoms as well as ten possible adsorption sites ($\mathbf{t_1}$–$\mathbf{t_4}$ and $\mathbf{b_1}$–$\mathbf{b_6}$). There are four types of surface atoms with different coordination patterns exposed on the surface. At the $\mathbf{t_2}$ site, the surface Mo_A atom coordinates with seven Mo atoms, and the surface Mo_B atom at the $\mathbf{t_4}$ site coordinates with eight Mo atoms. Both surface Mo atoms at the $\mathbf{t_2}$ and $\mathbf{t_4}$ sites coordinate with three C atoms and differ in the number of their coordinated Mo atoms. At the $\mathbf{t_1}$ site, the surface C_A atom coordinates with four Mo atoms and has two dangling bonds, and the surface C_B atom at the $\mathbf{t_3}$ site coordinates with five Mo atoms and has one dangling bond. Therefore, both C_A and Mo_A are coordinatively more unsaturated than C_B and Mo_B, respectively. For the bridge sites, the $\mathbf{b_1}$ site has two Mo_A atoms, the $\mathbf{b_2}$ site has two C_A atoms, the $\mathbf{b_3}$ site has two Mo_B atoms, the $\mathbf{b_4}$ site has one

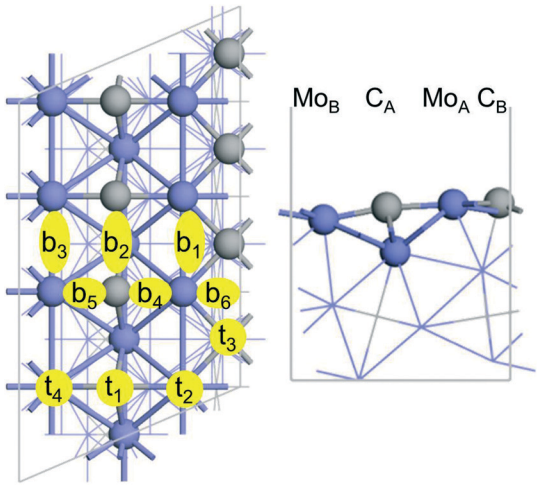

Fig. 1 Top and side views as well as possible adsorption sites of the Mo_2C(101) surface (Mo/blue, C/grey, b for bridge sites and t for top sites).

Mo_A and one C_A atom, the $\mathbf{b_5}$ site has one Mo_B and one C_A atom, and the $\mathbf{b_6}$ site has one Mo_A and one Mo_B atom.

3. Results and discussion

3.1 Molecular H_2O adsorption at different coverages (up to 1 ML)

On the (101) surface, the most stable adsorption configuration of one H_2O is located at the $\mathbf{t_2}$ site (−0.52 eV) with the O atom coordinating to one surface Mo_A atom, and the H_2O molecule stands parallel to the surface. All these are in agreement with previous studies.[53,54]

On the basis of this most stable adsorption configuration at the $\mathbf{t_2}$ site, we further identified the stable adsorption structures of H_2O at higher coverage. The selected structural parameters are listed in Table 1. The structures and stepwise adsorption energies of H_2O molecules at different coverages up to 1 ML (n = 1–8) are shown in Fig. 2. For n = 1–4, all H_2O molecules are adsorbed at the $\mathbf{t_2}$ sites on surface Mo_A atoms with steadily increased stepwise adsorption energies, which is associated with the H-bonding among the adsorbed H_2O molecules. The shortest H-bonding distance is found in the adsorption configuration with two H_2O molecules (1.876 Å), which is shorter than that in the gas phase (1.901 Å).[65] For n = 3 and 4, the H-bonding distances become longer (1.895/1.940 and 2.187/2.163/2.187/2.173 Å, respectively). It is noted that the distances between Mo and O atoms are in a close range (2.30–2.45 Å), indicating the coordination of the O atoms with the surface Mo_A atoms. For n = 4, all H_2O molecules arrange in a line interacting *via* H-bonding.

For n = 5–8, all H_2O molecules stand over the surface with H atoms pointing to the surface C_A atoms. The adsorbed H_2O molecules change the orientation of the previous linearly arranged adsorption of n = 4. For n = 7 and 8, one H_2O molecule stands over the surface with one H atom pointing to the surface Mo_B atom. The dominant interaction is H-bonding as indicated by the rather short distances (1.53–1.80 Å). The detailed H-bond arrangement is shown in Fig. S1.† On the basis of the Mo_A–O distances and the H-bonding distances, one can conclude that the dominant interaction is the coordination of O atoms with surface Mo_A atoms for n = 1–4, while the H-bonding interaction is dominant for n = 5–8. Nevertheless, their stepwise adsorption energies are very similar. It is also noted that one H_2O molecule is located over the Mo_A atom for n = 7 and 8. Nevertheless, the distances of H atoms to surface C_A or Mo_B atoms are rather long (>1.93 or >2.65 Å) and they do not show any significant interaction.

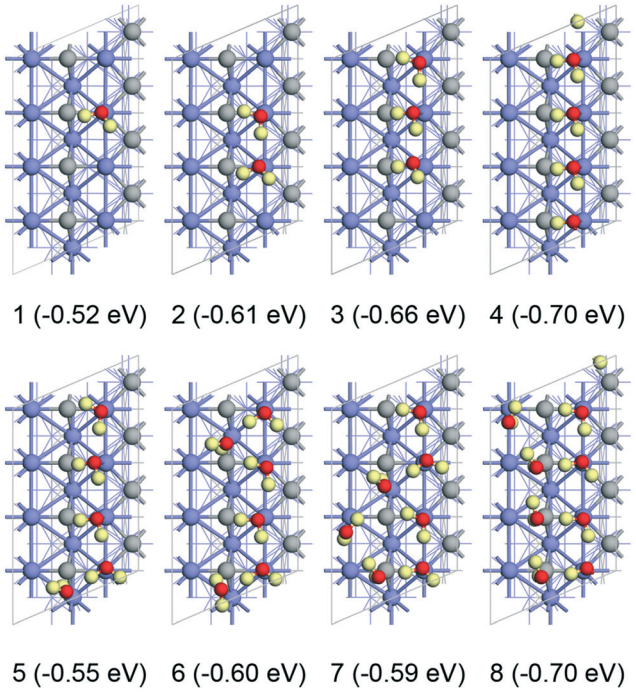

Fig. 2 Structures and stepwise adsorption energies of H_2O at different coverages on the Mo_2C(101) surface.

3.2 H_2O dissociation at different coverages

(a) H_2O direct dissociation. Previously, we found that, upon adsorption, molecular H_2O and surface O atoms prefer the top site of Mo_A atoms, surface OH groups prefer the bridge site between two Mo_A atoms, and surface H atoms prefer the top site of C_A atoms;[53,54] these are especially true for the dissociated states (ESI†). The other adsorption sites are energetically less favored. In this work, we used these most stable adsorption configurations to study H_2O dissociative adsorption, unless otherwise mentioned. On the basis of gaseous H_2O and H_2 as reference, the calculated adsorption energies of OH, H and O species are −1.10, −0.44 and −0.69 eV, respectively. In the sequential dissociation steps, the H atom from the previous step is considered to be released into the gas phase and therefore removed from the surface considering the next step.

Table 1 Selected distances (Å) on the Mo_2C(101) surface at different H_2O coverages

	$d_{\text{H-bond}}$ (Mo_A)	$d_{\text{Mo–O}}$ (Mo_A)	$d_{\text{H–C}}$ (C_A)
1H_2O (1/8 ML)		2.344	
2H_2O (1/4 ML)	1.876	2.327, 2.424	
3H_2O (3/8 ML)	1.895, 1.940	2.333, 2.414, 2.476	
4H_2O (1/2 ML)	2.187, 2.163, 2.187, 2.173	2.413, 2.415, 2.414, 2.145	
5H_2O (5/8 ML)	1.956, 2.319, 1.864, 1.896, 1.640	2.320, 2.431, 2.387, 2.391	1.960
6H_2O (3/4 ML)	2.085, 1.855, 1.801, 1.749, 1.557	2.352, 2.341, 2.369, 2.344	1.971, 2.024
7H_2O (7/8 ML)	1.770, 1.795, 1.784, 1.827, 2.011, 1.525	2.335, 2.368, 2.297, 2.347	1.971, 2.014
8H_2O (1 ML)	1.847, 1.856, 2.076, 1.621, 1.972, 1.636, 1.676, 1.956	2.327, 2.357, 2.285, 2.334	1.936, 2.000, 1.995

On the basis of the most stable H_2O adsorption configuration, we computed the dissociation of H_2O into surface H and OH as well as the successive dissociation of OH into O and H. The optimized geometries for the transition states are shown in Fig. 3, while the structures of the initial state (IS) and the final state (FS) are given in the ESI† (Fig. S2). The energetic data including dissociation barriers and reaction energies are listed in Table S1.† The corresponding potential energy surfaces (PES) are shown in Fig. 4. The first dissociation step [$H_2O \rightarrow OH + H$] has a low barrier (0.22 eV) and is highly exothermic (−0.96 eV). The breaking O–H distance in the transition state (**TS1**) is 1.318 Å. The second dissociation step [$OH \rightarrow O + H$] has a high barrier (0.74 eV) and is slightly exothermic (−0.16 eV). The breaking O–H distance in the transition state (**TS2**) is 1.324 Å. The energetic data indicate that surface OH and O might establish equilibrium depending on the hydrogenation conditions. The total H_2O dissociative adsorption ($H_2O \rightarrow O + 2H$) is exothermic by 1.18 eV. Without ZPE correction, these computed dissociation barriers and reaction energies are 0.39/0.90 and −0.96/−0.16 eV, which are in agreement with the previous data (0.37/0.89 and −0.96/−0.10 eV) without ZPE correction.[53,54]

(b) H_2O dissociative adsorption with co-adsorbed O. Since H_2O dissociation is very easy, co-adsorption of surface O should be possible; we considered the effect of co-adsorbed O atoms on H_2O dissociative adsorption. The structures of IS, TS and FS are given in the ESI† (Fig. S3). The co-adsorption energy of $O + H_2O$ is obtained using $E_{ads}(O + H_2O) = E(O + H_2O/slab) + E(H_2) - 2E(H_2O) - E(slab)$, where $E(O + H_2O/slab)$ is the total energy of the slab with co-adsorbed O atoms and H_2O molecules in its optimal geometry. Due to the possible H-bonding interaction, we used the closely co-adsorbed O and H_2O at the adjacent Mo_A top sites. In this co-adsorption configuration, the distance of H-bonding is 1.732 Å. The co-adsorption energy of $O + H_2O$ is −1.60 eV. As there are two different O–H bonds, we computed both routes. The dissociation of the O–H bond without H-bonding [$O + H_2O \rightarrow O + OH + H$] has a barrier of 0.54 eV and is exothermic by 0.57 eV. The breaking O–H distance in the transition state (**TS3**) is 1.344 Å. However, the dissociation [$O + H_2O \rightarrow 2OH$] of the O–H bond with H-bonding (disproportionation) has a lower barrier of 0.15 eV and is exothermic by 0.51 eV. The breaking O–H distance in the transition state (**TS4**) is 1.369 Å. These energetic data show that disproportionation is more favored kinetically than direct H_2O dissociation.

As these two OH groups are separated at two bridge sites (**IS5**), we calculated their dissociation one [$2OH \rightarrow O + H + OH$] by one [$O + OH \rightarrow 2O + H$]. Both OH dissociations have almost the same barriers (0.79/0.78 eV) and their reaction energy is 0.02 and −0.19 eV, respectively. The breaking O–H distance in the transition states (**TS5** and **TS6**) is 1.340 and 1.322 Å, respectively. These energetic data show that OH dissociation mediated by both co-adsorbed OH and O has higher barriers of 0.79/0.78 eV than the bare H_2O and OH dissociations. This reveals that the formation of 2OH from $O + H_2O$ disproportionation is more preferred kinetically and thermodynamically than further OH dissociation. Consequently, surface OH groups should be more abundant than surface O atoms. It is noted that OH adsorption at bridge sites is more stable than that at top sites by 0.45 eV for one OH adsorption. This site preference is also found for high coverage OH adsorption despite the H-bonding interaction at the neighboring top sites, *e.g.* 0.72, 0.82 and 0.62 eV for two, three and four OH adsorptions at bridge sites over top sites, respectively. This indicates that the H-bonding at top sites cannot compensate for the preferred energy difference of the bridge sites; therefore, we mainly considered the OH co-adsorption at bridge sites during the whole reaction process.

(c) H_2O dissociation at higher coverage. On the basis of the identified most stable molecular adsorption configurations at high coverage, coverage-dependent H_2O dissociation was also considered. We firstly investigated the stepwise dissociation of the first four H_2O molecules because of their direct interaction with surface Mo atoms. On the basis of numerous considered possibilities for each dissociation step at high coverage, we only showed the energetically most favored step. The optimized geometries for the transition states are shown in Fig. 5, while the structures of the initial states (IS) and the final states (FS) and the corresponding energetic data are given in the ESI† (Table S1, Fig. S4–S6). The corresponding potential energy surfaces (PES) are shown in Fig. 6.

Starting from the co-adsorption configuration of $2H_2O$ molecules with H-bonding, we considered the O–H dissociation of the H_2O molecule as an H-bonding acceptor. The

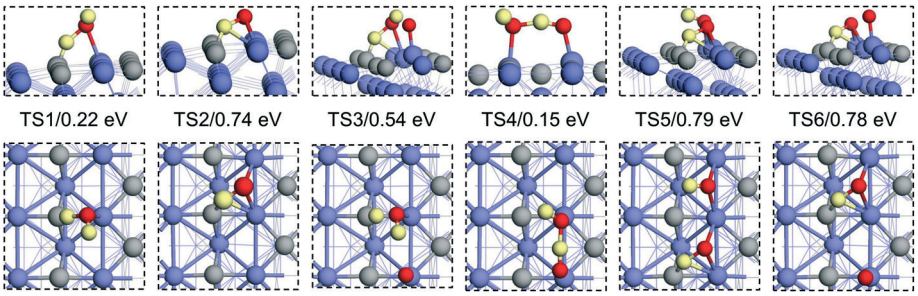

Fig. 3 Structures of transition states (TS) of H_2O and $O + H_2O$ dissociation on the $Mo_2C(101)$ surface.

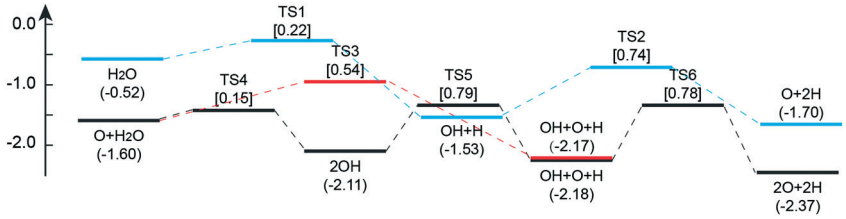

Fig. 4 Potential energy surfaces of H_2O and O + H_2O dissociation on the $Mo_2C(101)$ surface; the barriers of the elementary steps are given in square brackets.

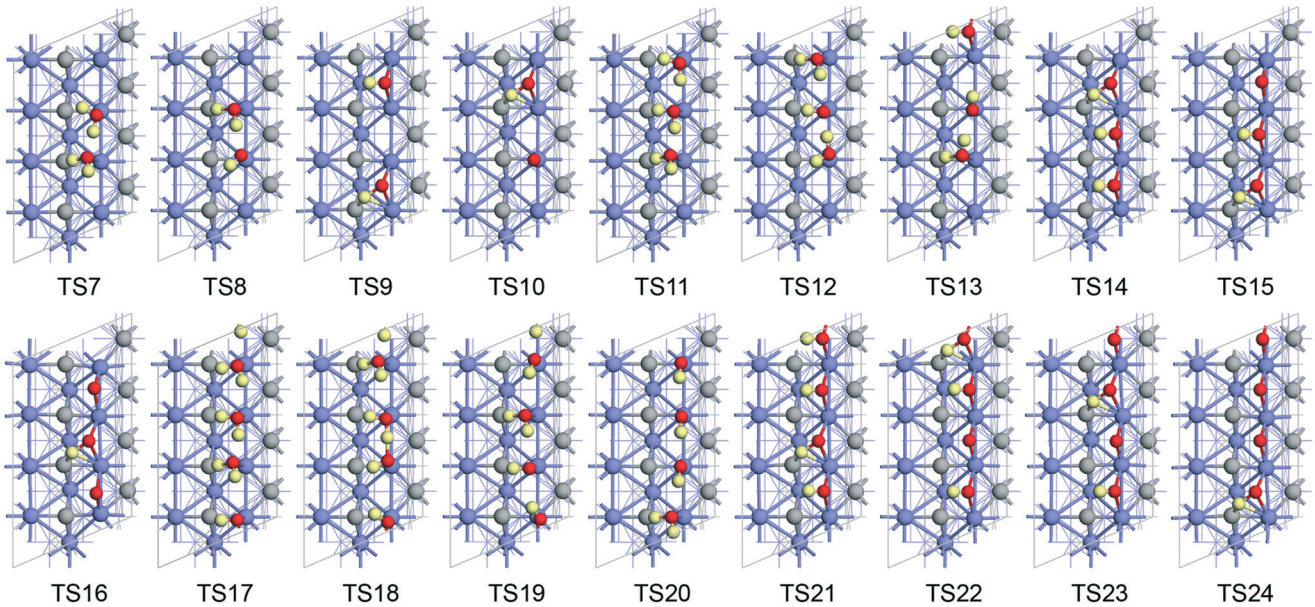

Fig. 5 Structures of transition states (TS) of nH_2O (n = 2–4) dissociation on the $Mo_2C(101)$ surface on the basis of H_2O dissociation and gaseous H_2 formation.

barrier is −0.11 eV (0.05 eV when excluding ZPE) and the dissociation is exothermic by 0.94 eV, indicating very facile and favored dissociation. As shown in Fig. 5, in the transition state (**TS7**), the breaking O–H distance is 1.232 Å and the H-bonding distance is 1.634 Å, shorter than that in the co-adsorbed initial state (1.876 Å). This strong H-bonding should be the driving force for the very low dissociation barrier. In the final state, H-bonding becomes even shorter (1.386 Å). The successive O–H dissociation has a barrier of 0.75 eV and is exothermic by 0.28 eV.

Alternatively, the O–H dissociation of the H_2O molecule as an H-bonding donor has a barrier of 0.59 eV and is exothermic by 0.91 eV. In the transition state (**TS8**), the breaking O–H distance is 1.347 Å and the H-bonding distance is 1.845 Å. These energetic data show that the co-adsorbed OH group suppresses H_2O dissociation kinetically compared with single H_2O dissociation (0.59 *vs.* 0.22 eV). In the final state, the two bridging OH groups are remote from each other with a very long distance between two O atoms (6.067 Å). Further dissociation of both these two OH groups has a barrier of 0.78 eV, and is slightly exothermic by 0.14 and 0.19 eV, respectively. In the transition states (**TS9** and **TS10**), the breaking O–H distance is 1.329 and 1.322 Å, respectively.

Starting from the co-adsorption configuration of $3H_2O$ molecules with H-bonding, the most favored first dissociation step is the O–H dissociation of the H_2O molecule acting only as an H-bonding acceptor. The barrier is −0.07 eV (0.09 eV when excluding ZPE) and the dissociation is exothermic by 1.07 eV. As shown in Fig. 5, in the transition state (**TS11**), the breaking O–H distance is 1.241 Å and the H-bonding distance is 1.958 and 1.711 Å. These results validate the strong H-bonding as the driving force for the low dissociation barrier. In the final state, the middle H_2O acting as both an H-bonding donor and acceptor transfers one proton to the just formed OH group by dissociation and forms two shorter H-bonds (1.656 and 1.641 Å). Indeed, this simultaneous proton transfer forms the new OH group in the middle site, and this OH acts as the acceptor of H-bonds from the two H_2O molecules both acting as H-bonding donors in the sides. The final effect is the dissociation of the central H_2O molecule acting as both an H-bonding donor and acceptor.

The next O–H dissociation of the H_2O molecule as an H-bonding donor has a barrier of 0.45 eV and is exothermic by 0.30 eV. In the transition state (**TS12**), the breaking O–H distance is 1.313 Å and the H-bonding distances change to

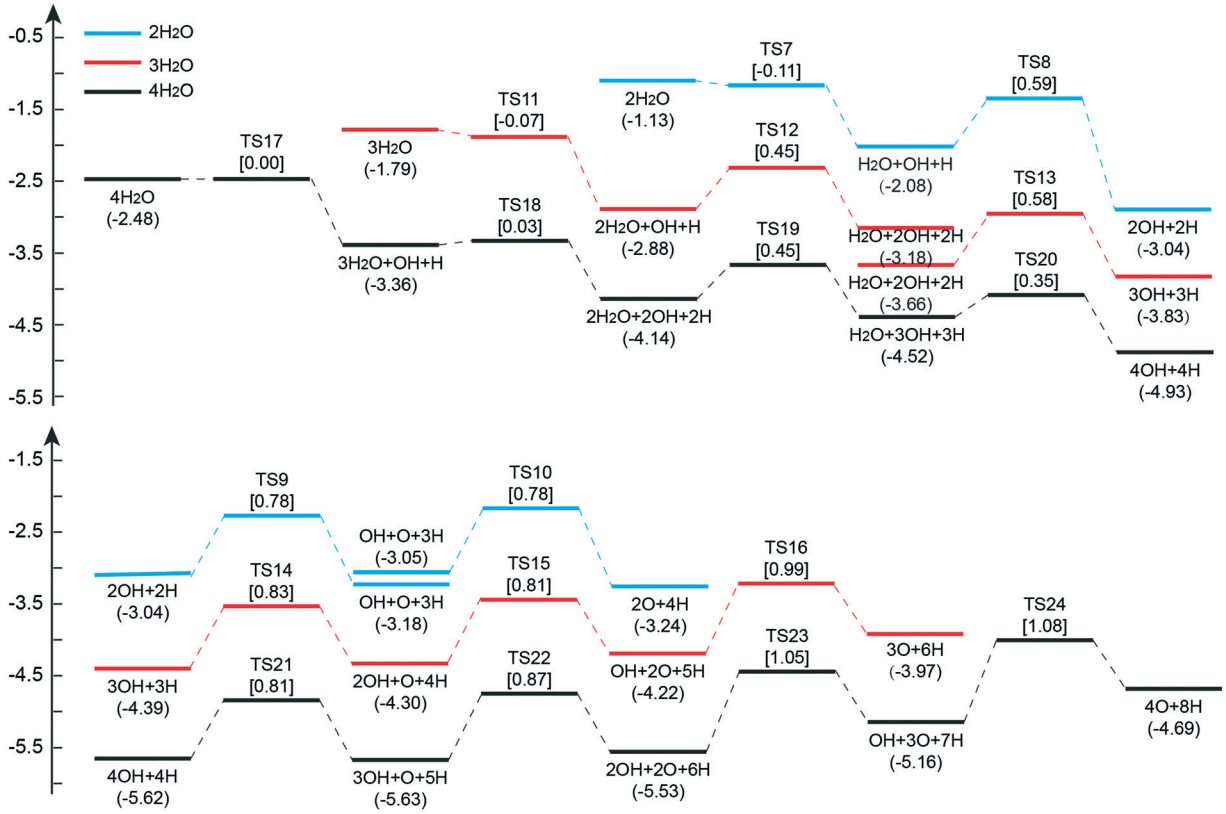

Fig. 6 Potential energy surfaces of nH_2O (n = 2–4) dissociation on the $Mo_2C(101)$ surface; the barriers of the elementary steps are given in square brackets.

2.281 and 1.498 Å, respectively. In the final state, the H-bonding distances change to 1.914 and 1.607 Å.

After removing the surface H atom, the OH group with longer H-bonding (1.914 Å) shifts from the top site to the bridge site, and the center OH group as well as the H_2O molecule acting as the H-donor (1.477 Å) is still at the top sites. The O–H dissociation of the last H_2O molecule has a barrier of 0.58 eV and is slightly exothermic by 0.17 eV. In the transition state (**TS13**), the breaking O–H distance is 1.326 Å and the H-bonding distance is elongated to 1.873 Å. In the final state, the H-bonding distance between two OH groups is 1.791 Å. As the OH group prefers the bridge site, the OH groups at the top sites migrate to the bridge sites and finally all three OH groups are parallel at the bridge sites without H-bonding; such migration is favored by 0.47 eV.

Further dissociation of the three bridged OH groups has barriers of 0.83, 0.81 and 0.99 eV, and is endothermic by 0.06, 0.13 and 0.25 eV, respectively. In the transition states (**TS14**, **TS15** and **TS16**), the breaking O–H distance is 1.325, 1.339 and 1.336 Å, respectively. The migration of these O atoms from the bridge sites to the top sites is favored by 0.17 eV in the final state.

Similar dissociation behaviors have been found for the four co-adsorbed H_2O molecules (Fig. S6†). As found for the dissociation of two and three H_2O molecules, the O–H dissociation of H_2O molecules has low barriers (0.00, 0.03, 0.45 and 0.35 eV, respectively) and is exothermic (−0.86, −0.77, −0.29 and −0.41 eV, respectively) due to the H-bonding. The dissociation of the four co-adsorbed OH groups has high barriers (0.81, 0.87, 1.05 and 1.08 eV, respectively) and is endothermic (0.66, 0.17, 0.42 and 0.46 eV, respectively). The migration of these O atoms from the bridge sites to the top sites is favored by 0.53 eV in the final state.

Based on the above discussed results, we can conclude that the dissociation of nH_2O (n = 2–4) into surface OH is very favorable both kinetically and thermodynamically, and this process is assisted by the formation of short H-bonds in the transition state while hindered by the elongation of H-bonds in the transition state. The energetic data for nOH dissociation also suggest that the O–H dissociation of the OH group is less favored than that of the H_2O molecule both kinetically and thermodynamically, and becomes more difficult when increasing the co-adsorbed coverage of O atoms.

Apart from the dissociation of these H_2O molecules interacting directly with surface Mo_A atoms (n = 1–4), we computed the dissociation of the H_2O molecule interacting with previously adsorbed H_2O *via* H-bonding (Fig. S7,† n = 5). However, this dissociation has a high barrier (0.63 eV) and is endothermic (0.41 eV), and the barrier is even higher than the corresponding desorption energy (negative stepwise adsorption energy, 0.55 eV). Obviously, at high coverage ($\theta >$ 0.5 ML), the dissociation of the four H_2O molecules interacting with surface Mo atoms is very favorable both kinetically and thermodynamically, while those H_2O molecules

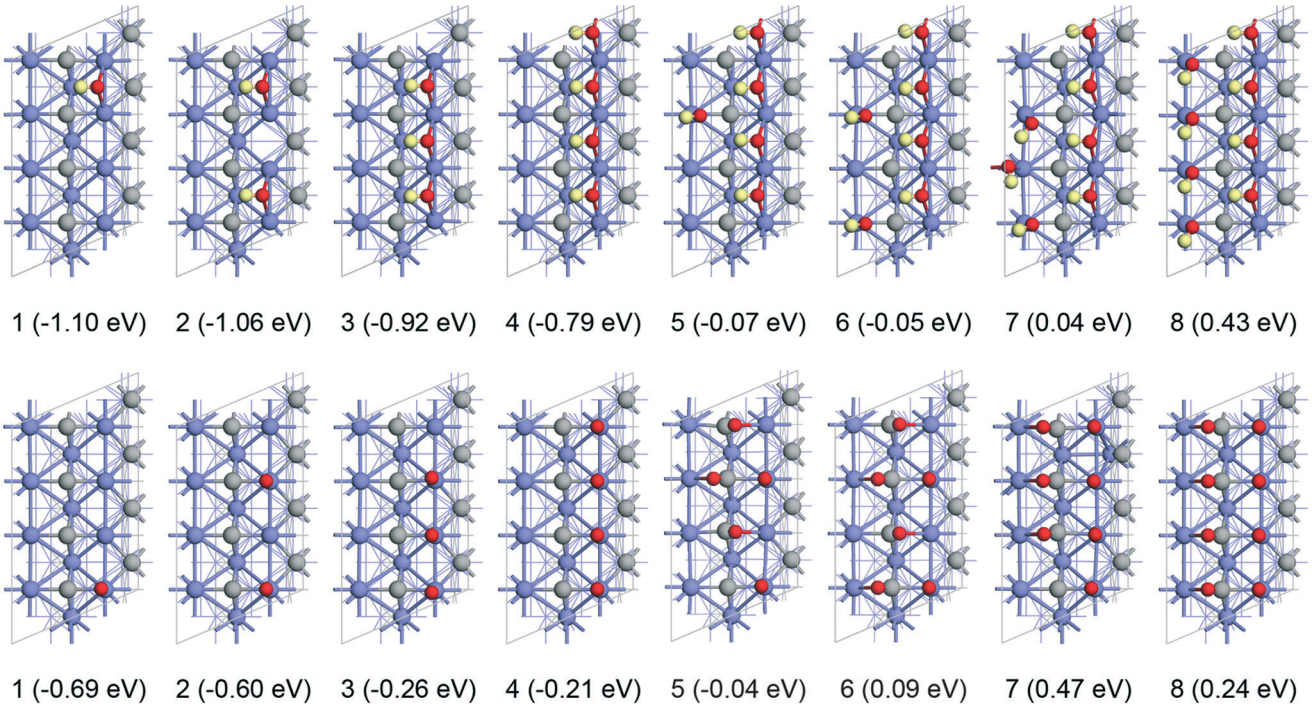

Fig. 7 Structures and stepwise adsorption energies of OH and O at different coverages on the $Mo_2C(101)$ surface on the basis of H_2O dissociation and gaseous H_2 formation.

interacting only by H-bonding prefer desorption rather than dissociation.

(d) Surface oxidation by H_2O. To understand surface oxidation by H_2O, we computed the adsorption of surface OH groups and O atoms at high coverage on the basis of gaseous H_2O and H_2. As shown in Fig. 7, the first four adsorbed OH groups (n = 1–4) are located at sites bridging two Mo_A atoms, and the stepwise adsorption energy decreases from −1.10 eV to −0.79 eV. However, the other four OH groups (n = 5–8) are at the top sites of the Mo_B atoms, and the stepwise adsorption energy is either close to zero (n = 5–7) or positive (0.43 eV, n = 8). Considering that desorption is easier than dissociation at $\theta > 0.5$ ML, one can conclude that this surface can only be oxidized at 0.5 ML OH coverage.

The stepwise adsorption energies of the first four O atoms (n = 1–4) are negative, and those of the first two O atoms are much higher than those of the third and fourth. Further increase of the oxygen coverage results in a large decrease of the stepwise adsorption energy, *i.e.*, close to zero for n = 5 and 6 and positive for n = 7 and 8. For the other two O atoms (n = 5 and 6), the O atoms are not regularly distributed on the surface, and they can also change the adsorption sites of the first four O atoms (n = 1–4). For n = 7 and 8, there are four O atoms at the top sites of Mo_A atoms and three or four O atoms at the bridging sites between C_A and Mo_B atoms. On the basis of the high OH dissociation barriers and the endothermic properties on the surfaces of OH + 2O and 2O + 2OH (Fig. 6), the surface O coverage cannot be higher than 0.25 ML.

On the basis of these data, one can clearly see that the first adsorption of surface O from the first surface OH dissociation is endothermic by 0.41 eV, which indicates that the adsorption of surface O is much less favored thermodynamically than that of surface OH; therefore, surface OH should be the most abundant species on the $Mo_2C(101)$ surface under an H_2O environment. Consequently, it is essential to consider the presence of surface OH instead of surface O during mechanism investigations on the Mo_2C catalyst, for example, in the hydrodeoxygenation of renewable biomass. These results may also explain why H_2O-pretreated Mo_2C catalysts have higher toluene synthesis rates than the O_2-pretreated one mentioned by Chen and Bhan.[31]

4. Conclusion

Periodic density functional theory calculations were performed to investigate the oxidation of the hexagonal $Mo_2C(101)$ surface by H_2O dissociative adsorption. It is found that the most stable adsorption of H_2O occurs at the $\mathbf{t_2}$ site with the O atom coordinating to the surface Mo_A atom. At the coverage up to 0.5 ML, all H_2O molecules adsorb at the $\mathbf{t_2}$ sites. For those H_2O molecules having direct interaction with the surface, their dissociation into surface OH is favorable both kinetically and thermodynamically, while the dissociation of OH into O + H can establish equilibrium. Moreover, surface O can easily react with H_2O to generate OH. At higher coverage ($\theta > 0.5$ ML), the added molecules adsorb only through H-bonding, and these H_2O molecules interacting only through H-bonding prefer desorption rather than dissociation. These results clearly reveal that OH is the most abundant oxygenate species on the $Mo_2C(101)$ surface, and the

highest coverage of OH is 0.5 ML. Surface OH instead of surface O atoms should play an essential role in mechanisms of many related reactions.

Acknowledgements

This work was supported by the National Natural Science Foundation of China (no. U1510103). The calculations were performed using supercomputers at the Supercomputing Center of Shanxi University.

References

1 L. E. Toth, *Transition Metal Carbides and Nitrides*, Academic Press, New York, 1971.
2 S. T. Oyama, *The Chemistry of Transition Metal Carbides and Nitrides*, Blackie Academic and Professional, Glasgow, 1996.
3 R. B. Levy and M. Boudart, *Science*, 1973, **181**, 547–549.
4 S. T. Oyama, *Catal. Today*, 1992, **15**, 179–200.
5 M. Nagai and K. Matsuda, *J. Catal.*, 2006, **238**, 489–496.
6 J. A. Schaidle, A. C. Lausche and L. T. Thompson, *J. Catal.*, 2010, **272**, 235–245.
7 M. K. Neylon, S. Choi, H. Kwon, K. E. Curry and L. T. Thompson, *Appl. Catal., A*, 1999, **183**, 253–263.
8 V. Sundaramurthy, A. K. Dalai and J. Adjaye, *Appl. Catal., B*, 2006, **68**, 38–48.
9 H. A. Al-Megren, S. L. Gonzalez-Cortes, T. C. Xiao and M. L. H. Green, *Appl. Catal., A*, 2007, **329**, 36–45.
10 R. Barthos and F. Solymosi, *J. Catal.*, 2007, **249**, 289–299.
11 S. Zaman and K. J. Smith, *Catal. Rev.: Sci. Eng.*, 2012, **54**, 41–132.
12 T. G. Kelly and J. G. Chen, *Green Chem.*, 2014, **16**, 777–784.
13 S. A. W. Hollak, R. W. Gosselink, D. S. van Es and J. H. Bitter, *ACS Catal.*, 2013, **3**, 2837–2844.
14 K. Xiong, W. T. Yu and J. G. Chen, *Appl. Surf. Sci.*, 2014, **323**, 88–95.
15 W. S. Lee, Z. S. Wang, W. Q. Zheng, D. G. Vlachos and A. Bhan, *Catal. Sci. Technol.*, 2014, **4**, 2340–2352.
16 K. Xiong, W. S. Lee, A. Bhan and J. G. Chen, *ChemSusChem*, 2014, **7**, 2146–2151.
17 H. Vrubel and X. Hu, *Angew. Chem.*, 2012, **124**, 12875–12878.
18 W.-F. Chen, C.-H. Wang, K. Sasaki, N. Marinkovic, W. Xu, J. T. Muckerman, Y. Zhu and R. R. Adzic, *Energy Environ. Sci.*, 2013, **6**, 943–951.
19 L. Liao, S. Wang, J. Xiao, X. Bian, Y. Zhang, M. D. Scanlon, X. Hu, Y. Tang, B. Liu and H. H. Girault, *Energy Environ. Sci.*, 2014, **7**, 387–392.
20 Y. Liu, G. Yu, G. Li, Y. Sun, T. Asefa, W. Chen and X. Zou, *Angew. Chem., Int. Ed.*, 2015, **54**, 10752–10757.
21 C. Wan, Y. N. Regmi and B. M. Leonard, *Angew. Chem., Int. Ed.*, 2014, **53**, 6407–6410.
22 S. Meyer, A. V. Nikiforov, I. M. Petrushina, K. Köhler, E. Christensen, J. O. Jensen and N. J. Bjerrum, *Int. J. Hydrogen Energy*, 2015, **40**, 2905–2911.
23 J. R. D. S. Politi, F. Vines, J. A. Rodriguez and F. IIIas, *Phys. Chem. Chem. Phys.*, 2013, **15**, 12617–12625.
24 J. A. Rodriguez and F. Illas, *Phys. Chem. Chem. Phys.*, 2012, **14**, 427–438.
25 J. A. Rodriguez, P. Liu, Y. Takahashi, F. Vines, L. Feria, E. Florez, K. Nakamura and F. Illas, *Catal. Today*, 2011, **166**, 2–9.
26 S. Posada-Pérez, P. J. Ramírez, J. Evans, F. Viñes, P. Liu, F. Illas and J. A. Rodriguez, *J. Am. Chem. Soc.*, 2016, **138**, 8269–8278.
27 S. Posada-Pérez, P. J. Ramírez, R. A. Gutiérrez, D. J. Stacchiola, F. Viñes, P. Liu, F. Illas and J. A. Rodriguez, *Catal. Sci. Technol.*, 2016, **6**, 6766–6777.
28 S. Posada-Pérez, F. Viñes, P. J. Ramírez, A. B. Vidal, J. A. Rodriguez and F. Illas, *Phys. Chem. Chem. Phys.*, 2014, **16**, 14912–14921.
29 X. Zhang, X. Zhu, L. Lin, S. Yao, M. Zhang, X. Liu, Y.-W. Li, C. Shi and D. Ma, *ACS Catal.*, 2017, **7**, 912–918.
30 W. Wu, Z. Wu, C. Liang, P. Ying, Z. Feng and C. Li, *Phys. Chem. Chem. Phys.*, 2004, **6**, 5603–5608.
31 C. J. Chen and A. Bhan, *ACS Catal.*, 2017, **7**, 1113–1122.
32 A. S. Rocha, A. B. Rocha and V. T. Silva, *Appl. Catal., A*, 2010, **379**, 54–60.
33 X. R. Shi, J. G. Wang and K. Hermann, *J. Phys. Chem. C*, 2010, **114**, 13630–13641.
34 T. Wang, S. G. Wang, Y. W. Li, J. G. Wang and H. Jiao, *J. Phys. Chem. C*, 2012, **116**, 6340–6348.
35 C. Pistonesi, M. E. Pronsato, L. Bugyi and A. Juan, *J. Phys. Chem. C*, 2012, **116**, 24573–24581.
36 T. Wang, Y.-W. Li, J. Wang, M. Beller and H. Jiao, *J. Phys. Chem. C*, 2014, **118**, 3162–3171.
37 T. Wang, Q. Luo, Y.-W. Li, J. Wang, M. Beller and H. Jiao, *Appl. Catal., A*, 2014, **478**, 146–156.
38 J. Ren, C. F. Huo, J. G. Wang, Z. Cao, Y. W. Li and H. Jiao, *Surf. Sci.*, 2006, **600**, 2329–2337.
39 T. Wang, Y.-W. Li, J. Wang, M. Beller and H. Jiao, *J. Phys. Chem. C*, 2014, **118**, 8079–8089.
40 T. Wang, X. X. Tian, Y. Yang, Y.-W. Li, J. Wang, M. Beller and H. Jiao, *Phys. Chem. Chem. Phys.*, 2015, **17**, 1907–1917.
41 T. Wang, X. X. Tian, Y.-W. Li, J. Wang, M. Beller and H. Jiao, *Surf. Sci.*, 2016, **651**, 195–202.
42 H. Tominaga and M. Nagai, *Appl. Catal., A*, 2008, **343**, 95–103.
43 A. Kotarba, G. Adamski, W. Piskorz, Z. Sojka, C. Sayag and G. Djega-Mariadassou, *J. Phys. Chem. B*, 2004, **108**, 2885–2892.
44 C. Pistonesi, A. Juan, A. P. Farkas and F. Solymosi, *Surf. Sci.*, 2008, **602**, 2206–2211.
45 M. E. Pronsato, C. Pistonesi, A. Juan, A. P. Farkas, L. Bugyi and F. Solymosi, *J. Phys. Chem. C*, 2011, **115**, 2798–2804.
46 P. Liu, J. A. Rodriguez and J. T. Muckerman, *J. Phys. Chem. B*, 2004, **108**, 15662–15670.
47 N. M. Schweitzer, J. A. Schaidle, O. K. Ezekoye, X. Q. Pan, S. Linic and L. T. Thompson, *J. Am. Chem. Soc.*, 2011, **133**, 2378–2381.
48 A. J. Medford, A. Vojvodic, F. Studt, F. Abild-Pedersen and J. K. Nørskov, *J. Catal.*, 2012, **290**, 108–117.
49 K. Z. Qi, G. C. Wang and W. J. Zheng, *Surf. Sci.*, 2013, **614**, 53–63.

50 Q. Q. Luo, T. Wang, G. Walther, M. Beller and H. Jiao, *J. Power Sources*, 2014, **246**, 548–555.
51 H. Tominaga and M. Nagai, *J. Phys. Chem. B*, 2005, **109**, 20415–20423.
52 P. Liu and J. A. Rodriguez, *J. Phys. Chem. B*, 2006, **110**, 19418–19425.
53 Y. Shi, Y. Yang, Y.-W. Li and H. Jiao, *Appl. Catal., A*, 2016, **524**, 223–236.
54 Y. Shi, Y. Yang, Y.-W. Li and H. Jiao, *Catal. Sci. Technol.*, 2016, **6**, 4923–4936.
55 Y. Shi, Y. Yang, Y.-W. Li and H. Jiao, *ACS Catal.*, 2016, **6**, 6790–6803.
56 G. Kresse and J. Furthmüller, *Comput. Mater. Sci.*, 1996, **6**, 15–50.
57 G. Kresse and J. Furthmüller, *J. Phys. Rev. B*, 1996, **54**, 11169–11186.
58 P. E. Blochl, *Phys. Rev. B: Condens. Matter Mater. Phys.*, 1994, **50**, 17953–17979.
59 G. Kresse, *Phys. Rev. B: Condens. Matter Mater. Phys.*, 1999, **59**, 1758–1775.
60 J. P. Perdew, K. Burke and M. Ernzerhof, *Phys. Rev. Lett.*, 1996, **77**, 3865–3868.
61 G. Henkelman and H. Jónsson, *J. Chem. Phys.*, 2000, **113**, 9978–9985.
62 E. Parthe and V. Sadagopan, *Acta Crystallogr.*, 1963, **16**, 202–205.
63 T. Wang, X. W. Liu, S. G. Wang, C. F. Huo, Y. W. Li, J. G. Wang and H. Jiao, *J. Phys. Chem. C*, 2011, **115**, 22360–22368.
64 E. Rudy, S. Windisch, A. J. Stosick and J. R. Hoffman, *Trans. Metall. Soc. AIME*, 1967, **239**, 1247–1249.
65 S. Liu, X. X. Tian, T. Wang, X. D. Wen, Y.-W. Li, J. Wang and H. Jiao, *J. Phys. Chem. C*, 2014, **118**, 26139–26154.